Supporting Information

Inter-regulated *d*-band centers of Ni_3B/Ni heterostructure for boosting hydrogen electrooxidation in alkaline media

Fulin Yang,[†a] Pengyu Han,[†a] Na Yao,[†a] Gongzhen Cheng,[a] Shengli Chen[a] and Wei Luo*[a]

[a]College of Chemistry and Molecular Sciences, Wuhan University, Wuhan, Hubei 430072, P. R. China, Tel.: +86-027-68752366

*Corresponding author. E-mail addresses: wluo@whu.edu.cn.

[†]These authors contributed equally.

Experimental Procedures

Chemicals

All chemicals were used as received without any further purification. Nickel (II) chloride hexahydrate ($NiCl_2 \cdot 6H_2O$, Sinopharm Chemical Reagent Co. Ltd., AR), sodium borohydride ($NaBH_4$, Linfeng Chemical Reagent (Shanghai) Co. Ltd., AR), sodium hydroxide (NaOH, Sinopharm Chemical Reagent Co. Ltd., AR), potassium hydroxide (KOH, Sinopharm Chemical Reagent Co. Ltd., 85.0%), isopropyl alcohol (C_3H_8O, Sinopharm Chemical Reagent Co. Ltd, 99.7%), Nafion solution (Sigma-Aldrich Co., 5 wt%). The ultrapure water (18.25 MΩ cm^{-1}) was used throughout the whole experiment.

Syntheses of amorphous Ni-B precursor

Amorphous Ni-B precursor was synthesized via a conventional reduction method.[1,2] In a typical synthesis, $NiCl_2 \cdot 6H_2O$ (2.377 g) was dissolved in 20 mL of deionized water in a 100 mL three-necked round-bottomed flask and stirred under N_2 for 10 min to remove the air. Then, 0.945 g $NaBH_4$ and 80 mg NaOH was dissolved into 20 ml DI water and stirring 10 min to get $NaBH_4$ solution. Subsequently, $NaBH_4$ solution was added into $NiCl_2$ solution by slowly injection under ice-bath and nitrogen atmosphere. Immediate formation of a black precipitate was observed under continuous stirring. After 2 h, the as-prepared precipitate was collected via centrifugation at a speed of 5,000 rpm and further washed with DI water and ethanol for 3 times, then dried in a vacuum oven overnight at 60 °C.

Syntheses of NiB-*T* (*T* = 200, 300, or 400)

In a typical synthesis of NiB-*T*, 50mg of as-prepared amorphous Ni-B precursor was put into a crucible and placed in the center of pipe furnace. The furnace was filled with mixture of gases (95% Nitrogen

and 5% Hydrogen), and then heated to 200/300/400 °C with a ramp rate of 5 °C/min. After reacting 3 h, the furnace was cooled down to room temperature naturally. The precipitate was collected and denoted as NiB-*T* (*T* = 200, 300, or 400).

Synthesis of Ni

The Ni was synthesized by a modifying previous method.[3] 0.238 g $NiCl_2 \cdot 6H_2O$ was dissolved in 10 mL ice-cold water in a 50 mL round-bottom flask. Then, 10 mL ice-cold water solution containing 94.5 mg $NaBH_4$ was added dropwise into the $NiCl_2$ solution. The solution was stirred vigorously under ice-bath for 2 h, and then 1 mL 1 M KOH solution and 0.4 mL $N_2H_4 \cdot H_2O$ were added. The solution was transferred into a 25 mL autoclave and heated to 150 °C. After holding at 150 °C for 4 h, the autoclave was cooled down to room temperature. The precipitate was collected via centrifugation and washed with H_2O and ethanol for 3 times, then dried in a vacuum oven overnight at 60 °C.

Synthesis of Ni_3B

The Ni_3B was prepared according to the previous literature.[4] The synthesis was carried out in a 100 mL three-necked round-bottomed flask, into which 30 mL of TEG and 238 mg (1mmol) of nickel chloride were added. The solution was sonicated for 30 minutes to dissolve the salt and then allowed to stir and heat to about 45 °C on a heating mantle while purging with Ar. Then, a previously freshly prepared and chilled solution of 30 mL of TEG and 945 mg (25 mmol) of $NaBH_4$ was added dropwise to $NiCl_2$ solution with continuous stirring under Ar atmosphere. The metal salt solution was turned black quickly, which suggests the Ni^{2+} was reduced to zero-valent Ni^0 particles. When the $NaBH_4$ solution was dropped over, the mixture temperature was slowly ramped up to 280 °C, at which point

the temperature was held for 5 min. After that, the flask was removed from the heating mantle and allowed it to cool to room temperature. The product was collected by centrifugation and washing with ethanol until the supernatant is clear, indicating the residual TEG and byproducts was removed. The product was dried in a vacuum oven overnight at 60 °C finally.

Synthesis of Ni_3B-300

The Ni_3B-300 was synthesized via annealing treatment, 50mg of as-prepared Ni_3B was put into a crucible and placed in the center of pipe furnace. The furnace was filled with mixture of gases (95% Nitrogen and 5% Hydrogen), and then heated to 300 °C with a ramp rate of 5 °C/min. After 3 hours annealing, the furnace was cooled down to room temperature naturally and collected, which was denoted as Ni_3B-300.

Physical characterization

Powder X-ray diffraction (PXRD) patterns were performed on a Rigaku Miniflex600 X-ray powder diffractometer using a Cu Kα radiation source (λ = 0.154178 nm). All of the diffraction data were collected in a 2θ range from 10° to 80° at a scanning rate of 8° min^{-1}. The transmission electron microscopy (TEM) observation and the energy dispersive spectroscopy (EDS) data were performed using a FEI Tecnai G20 U-Twin transmission electron microscope equipped with an EDX spectrometer at an acceleration voltage of 200 kV. High resolution TEM (HRTEM) images and high angle annular dark field scanning transmission electron microscopy (HAADF-STEM) images were obtained on a Titan G2 60-300 transmission electron microscope operated at an acceleration voltage of 300 kV. The X-ray photoelectron spectroscopy (XPS) measurement was carried out in a Thermo

Fischer ESCALAB 250Xi spectrophotometer. The ultraviolet photoelectron spectroscopy (UPS) analysis of Ni, NiB-300, and Ni_3B were performed on a Thermo Fischer ESCALAB 250Xi spectrophotometer and the base pressure in the measurement chamber is lower 1×10^{-8} bar. Elemental analysis was performed using atomic absorption spectroscopy and inductively coupled plasma atomic emission spectroscopy (ICP-AES).

Preparation of working electrodes

The working electrode was prepared as followed: 2.5 mg sample and 2.5 mg XC-72 were dispersed in1.0 mL solvent of isopropyl alcohol containing 0.05 wt. % Nafion and then ultrasonicated for at least 30 min to form a homogeneous ink. The glassy-carbon electrode (GCE, 5 mm in diameter) was polished with 1.0, 0.5 and 0.05 μm alumina powder successively to obtain a mirrorlike surface and then washed with ultrapure water and ethanol with sonication. After the GCE was dried in air, 12 μL of the ink was drop-casted on the surface of the GCE intermittently (total loading 0.306 mg cm^{-2}) and dried in air before any electrochemical measurements. The loadings of Ni on electrocatalysts decorated electrodes could be calculated from the ICP-AES data, and are listed in Table S1 respectively.

Electrochemical Measurements

Electrochemical measurements were performed on a CHI 760E electrochemical analyzer (CH Instruments, Chenhua Co., Shanghai, China) in a conventional one-component three-electrode cell by using the modified GCE with various catalyst samples as the working electrodes, a Hg/HgO electrode (full filled with 0.1 M KOH) as the reference electrode and the graphite rod (diameter of 5 mm) as the counter electrode. In this work, all the measured potentials were referred to the reversible hydrogen

electrode (RHE) potential. For each electrochemical test, fresh 0.1 M potassium hydroxide (KOH) solution was employed as the electrolyte. Before hydrogen oxidation reaction (HOR) evaluation, we stabilized the GC disk surface at open circuit potential for more than 300 s in H_2-saturated 0.1 M KOH solution. Then, the polarization curves were recorded by a rotating disk electrode (RDE) system (Pine Research Instruments) with the rotation rate of 2500 revolutions per minute (rpm). The potential was scanned from -0.08 V to 0.12 V (vs. RHE) at a scan rate of 5 $mV \cdot s^{-1}$.

Electrochemically active surface areas (ECSAs) were determined by cyclic voltammetry that conducted in an Ar-saturated electrolyte. The potential window was selected between -0.13 and 0.52 V at the scan rate of 50 $mV \cdot s^{-1}$. The value of ECSA ($cm_{metal}\ \mu g_{metal}^{-1}$) can be calculated via Eq.S1,[3]

$$ECSA = \frac{Q_{Ni}}{Q_s \cdot m_{Ni}} \quad \text{Eq.S1}$$

where Q_{Ni} is the measured integral charge that corresponds the area of the shaded area as shown in Fig. SX, Q_s is the surface charge density of 514 $\mu C\ cm_{Ni}^{-2}$ which is assumed for one monolayer of OH adsorption on Ni, m_{Ni} is the mass of the Ni on GC.

Electrochemical impedance spectra (EIS) tests was carried out after each RDE measurement with the AC impedance spectra from 200 kHz to 0.1 kHz and a voltage perturbation of 5 mV. The real part of the resistance at 1 kHz was taken as the uncompensated resistance (R_u)[5] and was used to obtain the iR-free potential ($E_{iR\text{-}free}$) according to the following equation, Eq.S2,

$$E_{iR-free} = E - iR_u \quad \text{Eq.S2}$$

where *E* is the measured potential and i is the corresponding current.

Kinetic current density (j_k) could be extracted from the Koutecky–Levich equation (Eq.S3),[5]

$$\frac{1}{j} = \frac{1}{j_k} + \frac{1}{j_d} = \frac{1}{j_k} + \frac{1}{BC_0\omega^{1/2}} \quad \text{Eq.S3}$$

where j, j_d, B, c_0, and ω are the measured current density, the diffusion limited current density, the Levich constant, the solubility of H_2 (7.33×10^{-4} mol L^{-1}), and the speed of the rotating speed, respectively. Among them, B could be calculated from Eq. S4,[5]

$$B = 0.2nFD^{2/3}\nu^{-1/6} \quad \text{Eq. S4}$$

where n, F, D, and ν are the number of electrons transferred (2), the Faraday constant (96485 C mol^{-1}), the diffusivity of H_2 (3.7×10^{-5} cm^2 s^{-1}), and the kinematic viscosity (1.01×10^{-2} cm^2 s^{-1}), respectively.

Exchange current density (j_0), often used to evaluate the intrinsic activity of a catalyst, could be deduced from the Butler–Volmer equation (Eq.S5),[5]

$$j_k = j_0[e^{\frac{\alpha F}{RT}\eta} - e^{\frac{-(1-\alpha)F}{RT}\eta}] \quad \text{Eq.S5}$$

where α, R, T, and η represent the transfer coefficient, the universal gas constant (8.314 J mol^{-1} K^{-1}), the operating temperature (303 K in this work), and the overpotential, respectively.

The stability of NiB-300 catalyst was evaluated by the accelerated durability tests by scanning the potential between -0.08 and 0.42 V for 1000 cycles at the scanning rate of 100 mV s^{-1}.

CO-tolerance test was performed using the same electrochemical measurements of HOR test. The working electrode were prepared by 5 μL of 20wt% Pt/C ink dropping onto the RDE electrode to

achieve catalyst loading of 10 μg_{Pt} cm^{-2} (NiB-300 keep the same loading as the former test). The long-term stability tests were performed using chronoamperometry conducted in 0.1 M KOH saturated with CO containing (100 ppm) H_2 and measured at 0.05 V for more than 1 h. Before and after stability test, the linear sweep voltammetry (LSV) curves were carried out in 0.1 M KOH saturated with H_2 with the rotation rate of 2500 rpm (1600 rpm for Pt/C) and the potential was scanned from -0.08 V to 0.12 at a scan rate of 5 $mV \cdot s^{-1}$.

DFT Calculation Method

All spin-polarized calculations were based on periodic DFT with the Perdew-Burke-Ernzerhof (PBE) generalized gradient corrected approximation (GGA) for the exchange and correction functional in the framework of ultrasoft pseudopotentials and plane waves on CASTEP code of the Materials Studio package of Accelrys Inc. A kinetic energy cutoff of 370 eV for wave functions were used and the self-consistent field (SCF) tolerance was 1×10^{-6} eV. The crystal structures of Ni metal and Ni_3B are shown in Figure S18. Both for modeling Ni (111) and Ni_3B (001), periodically repeated three-layers slabs are used, and a vacuum layer of 15 Å along the *z*-direction is applied to separate the slabs, shown in Figures 1b and 1c. According to our experiments, the geometry optimization for Ni (111) and Ni_3B (001). To model the Ni_3B/Ni, we build the layered model (Figure 4b) to investigate the interaction effect between Ni and Ni_3B, and the enhance mechanism of HOR performance on such hybrid catalyst. The Brillouin-zones sampling for all calculations was performed with a 3 × 3 × 1 *k*-points mesh. The adsorption free energy of hydrogen (ΔG_{H^*}) is calculated by $\Delta G_{H^*} = \Delta E_{H^*} + \Delta ZPE - T\Delta S$, and the adsorption free energy of OH (ΔG_{OH^*}) is calculated by $\Delta G_{OH^*} = \Delta E_{OH^*} + \Delta ZPE - T\Delta S$, where ΔE_{H^*} and ΔE_{OH^*} are the DFT based adsorption energy of H or OH, ΔZPE and $T\Delta S$ are the correction of zero point energy

and entropy, respectively. E_{OH} is the energy of OH groups with reference to H_2O and H_2: $E_{OH} = E_{H2O} - 1/2E_{H_2}$. The related zero point energies and entropies of H_2, H_2O and H* are from previous DFT work. All the models with adsorbed species are exhibited in Figures S19-S22, and the data are shown in Tables S4 and S5. The site with the lowest energy among these sites was chosen for comparison in Figures 4f and 4g, which represents the most energetically stable sites.[6,7]

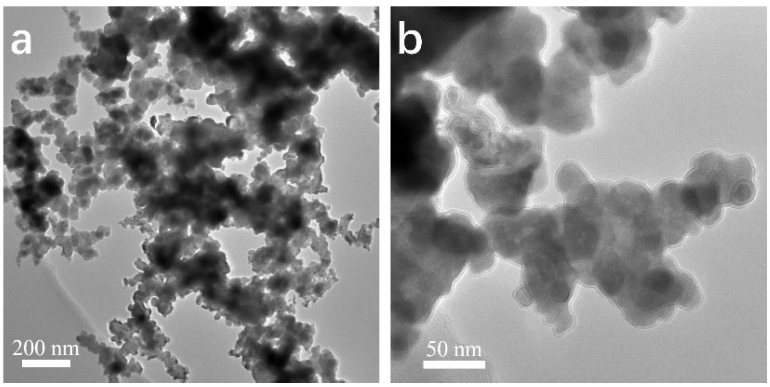

Fig. S1 TEM images of amorphous Ni-B precursor.

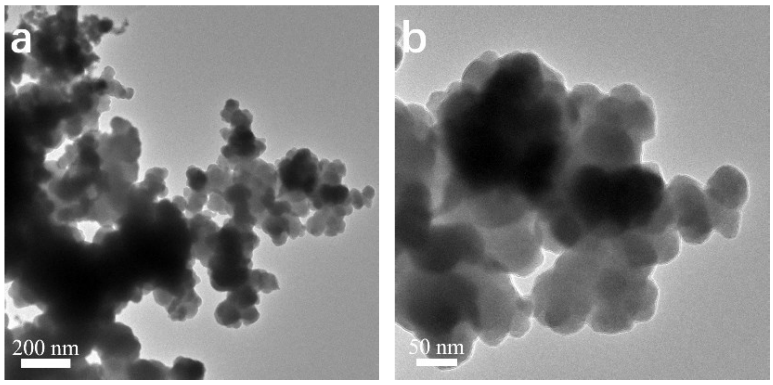

Fig. S2 TEM images of NiB-200.

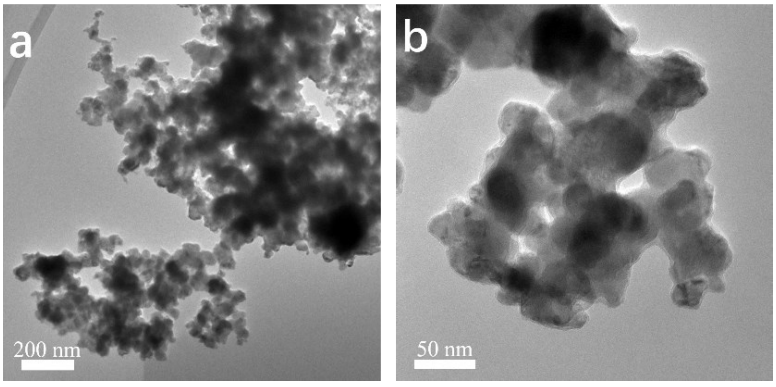

Fig. S3 TEM images of NiB-300.

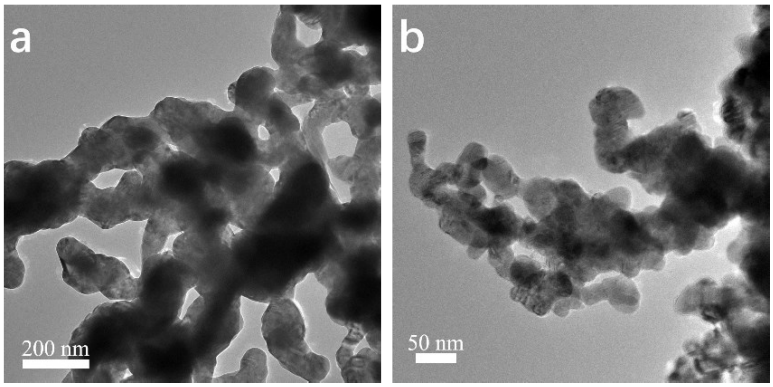

Fig. S4 TEM images of NiB-400.

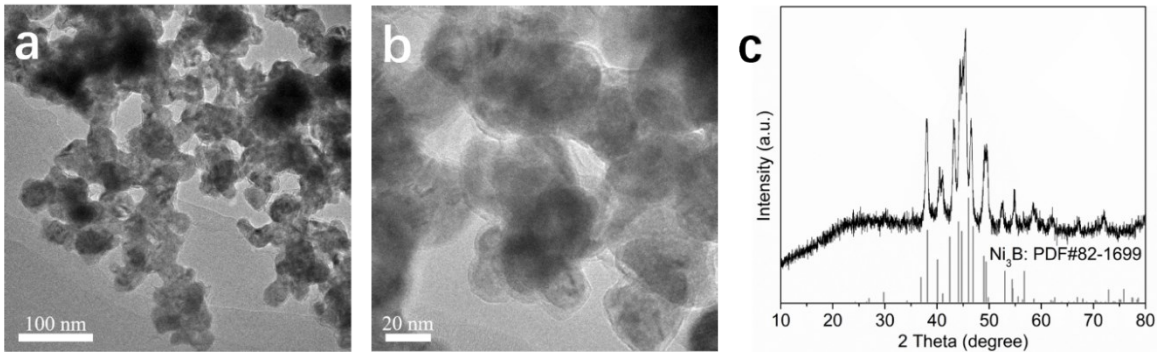

Fig. S5 TEM images (a, b) and XRD pattern (d) of Ni_3B.

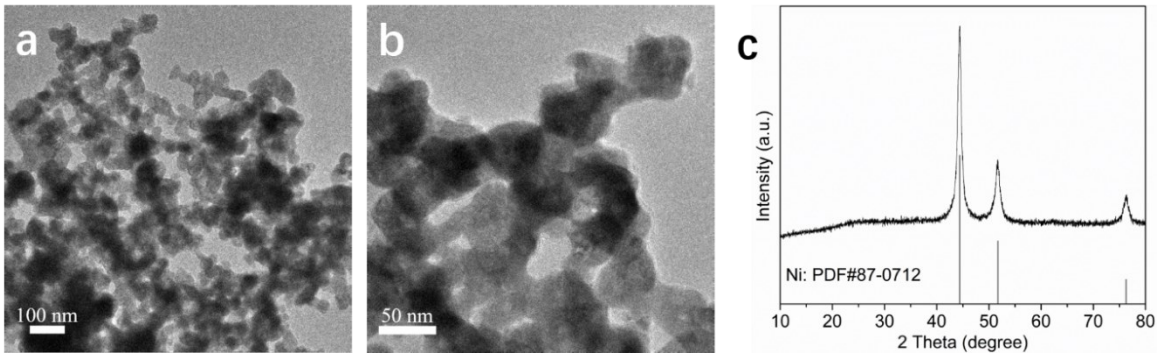

Fig. S6 TEM images (a, b) and XRD pattern (c) of Ni.

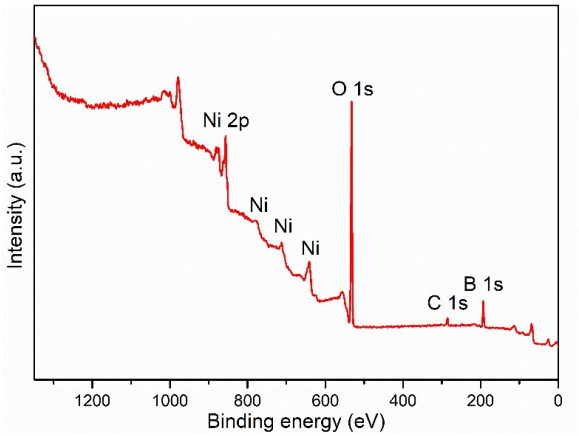

Fig. S7 XPS survey spectrum of NiB-300.

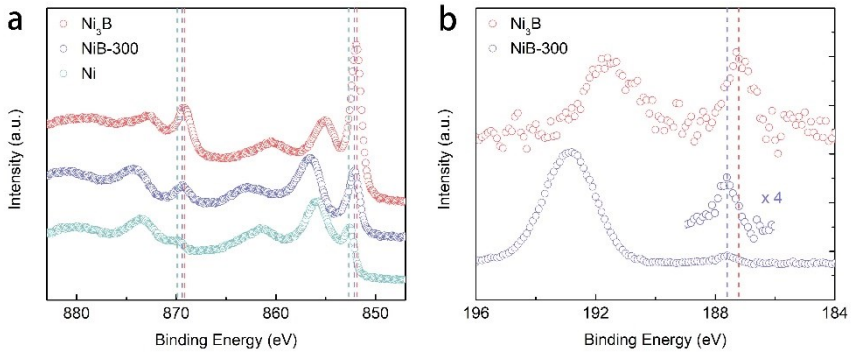

Fig. S8 (a) High-resolution Ni 2p XPS spectra of Ni, NiB-300, and Ni_3B; (b) High-resolution B 1s XPS spectra of NiB-300 and Ni_3B.

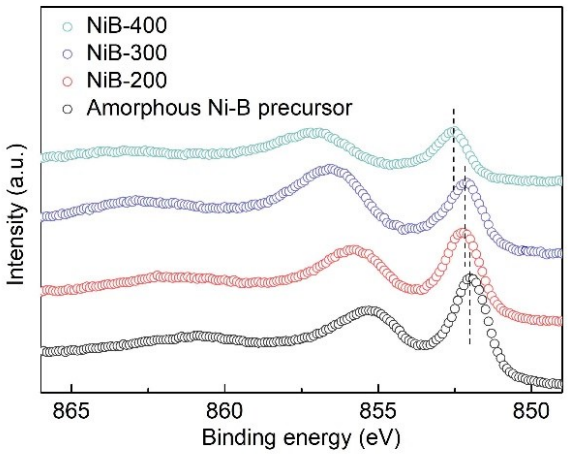

Fig. S9 High-resolution Ni $2p_{3/2}$ XPS spectra of amorphous Ni-B precursor, NiB-200, NiB-300, and NiB-400.

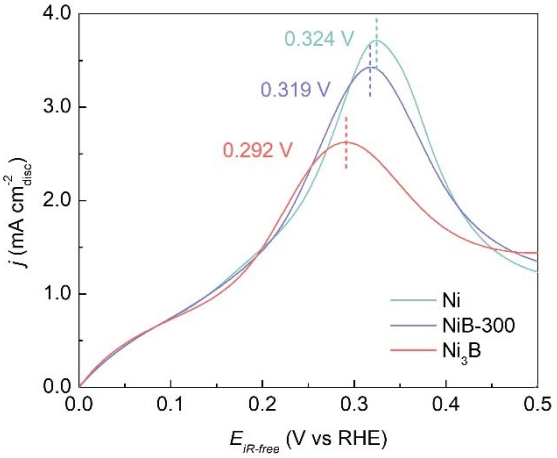

Fig. S10 Anodic polarization curves of Ni, Ni_3B, and Ni_3B-300 in Ar-saturated 0.1 M KOH at a scan rate of 50 mV s^{-1}.

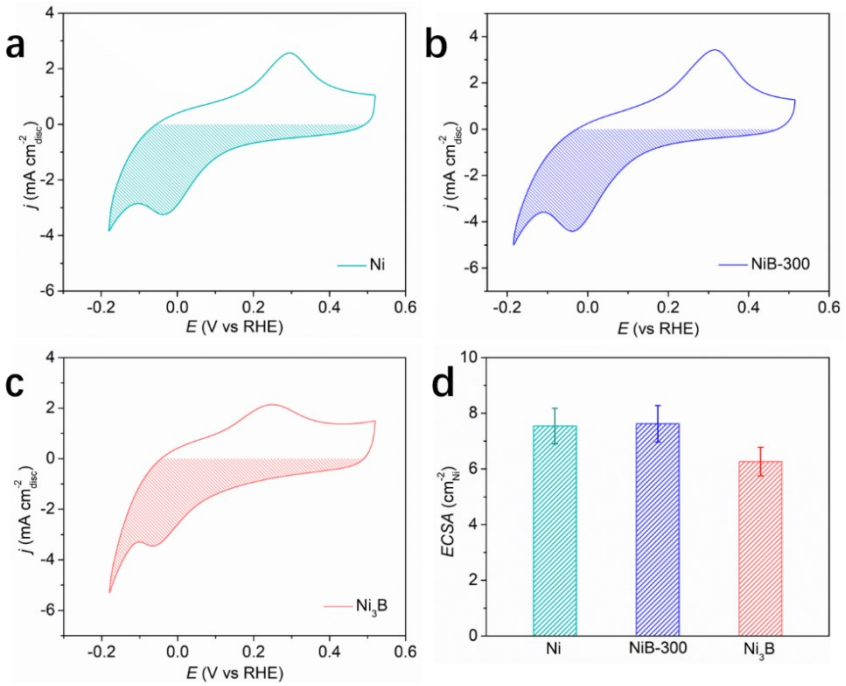

Fig. S11 CVs of (a) Ni, (b) NiB-300, and (c) Ni_3B in Ar-saturated 0.1 M KOH at a scan speed of 50 mV s^{-1}. The integral charges assigned as the patterned areas are used to estimate the ECSA with a charge density of 514 μC cm_{Ni}^{-2} for monolayer of OH adsorption on the surface of Ni. (d) Comparison of the ECSAs of the three catalysts.

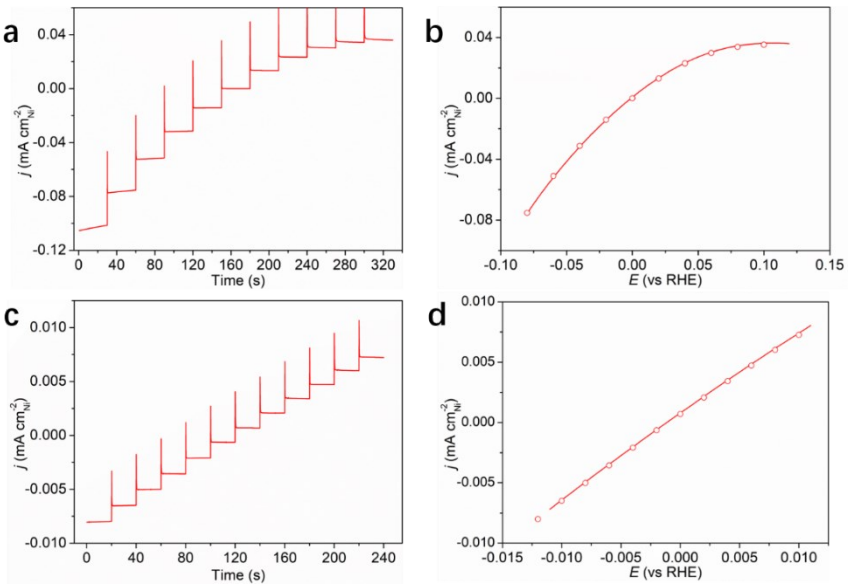

Fig. S12 Electrochemical activity measurements of NiB-300 in H_2-saturated 0.1 M KOH at 2500 rpm. (a) Current density vs. time response of NiB-300 to the potential program applied with the potential step of 20 mV. (b) Steady-state polarization curve (circle) and the corresponding transient polarization curve (line) obtained by LSV. (c) Current density vs. time response of NiB-300 to the potential program applied with the potential step of 2 mV. (b) Steady-state polarization curve (circle) and the corresponding transient polarization curve (line) obtained by LSV at the micropolarization regions. The potentials were *iR* uncorrected.

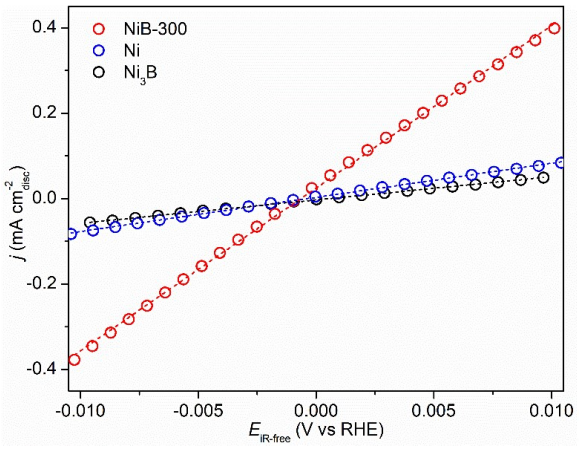

Fig. S13 Micropolarization region (−10 to 10 mV) of Ni, NiB-300, and Ni_3B in H_2-saturated 0.1 M KOH. The dashed lines indicate the linear fittings. All the potentials are iR-corrected.

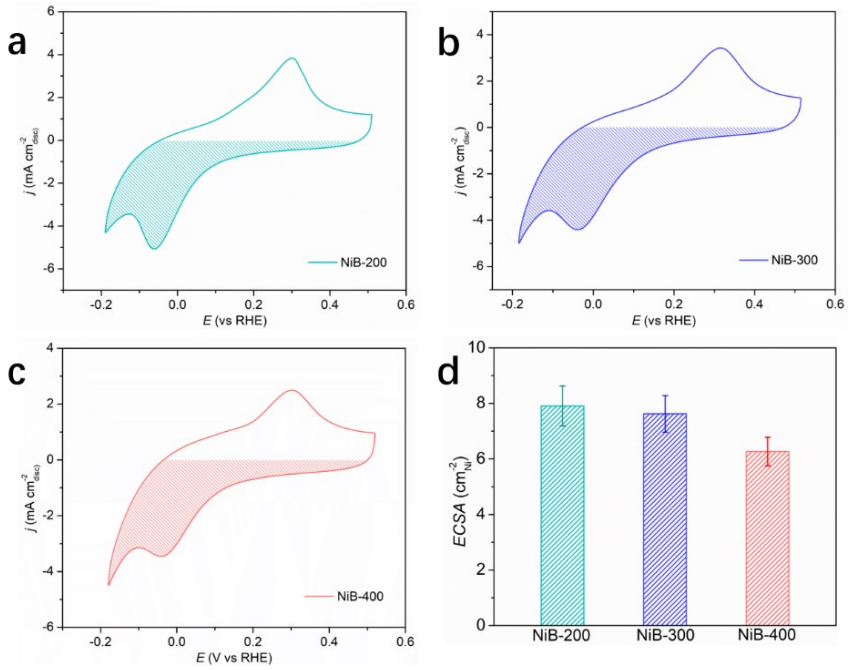

Fig. S14 CVs of (a) NiB-200, (b) NiB-300, and (c) NiB-400 in Ar-saturated 0.1 M KOH at a scan speed of 50 mV s^{-1}. The integral charges assigned as the patterned areas are used to estimate the ECSA with a charge density of 514 μC cm_{Ni}^{-2} for monolayer of OH adsorption on the surface of Ni. (d) Comparison of the ECSAs of the three catalysts.

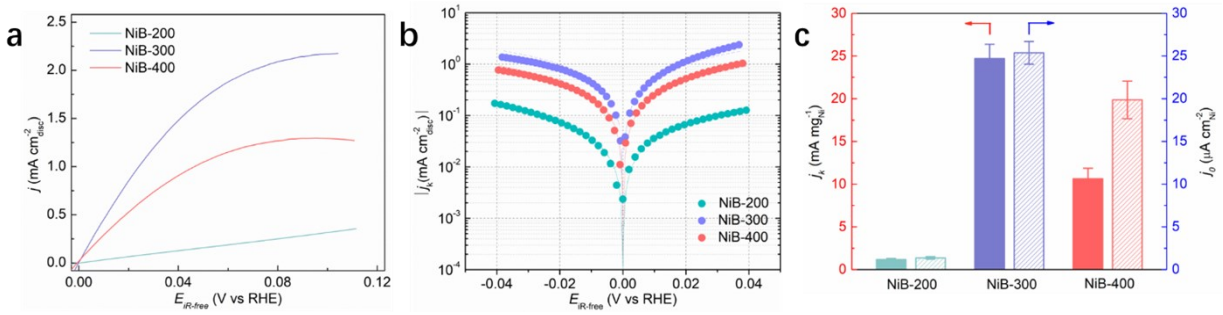

Fig. S15 (a) HOR polarization curves of NiB-200, NiB-300, and NiB-400 recorded in H_2-saturated 0.1 M KOH at a scan rate of 5 mV s^{-1} and a rotating speed of 2500 rpm; (b) Tafel plots derived from (a) as well as the corresponding fits to the Butler–Volmer equation; (c) Comparison of j_k and j_0 of Ni, Ni_3B and Ni_3B-300.

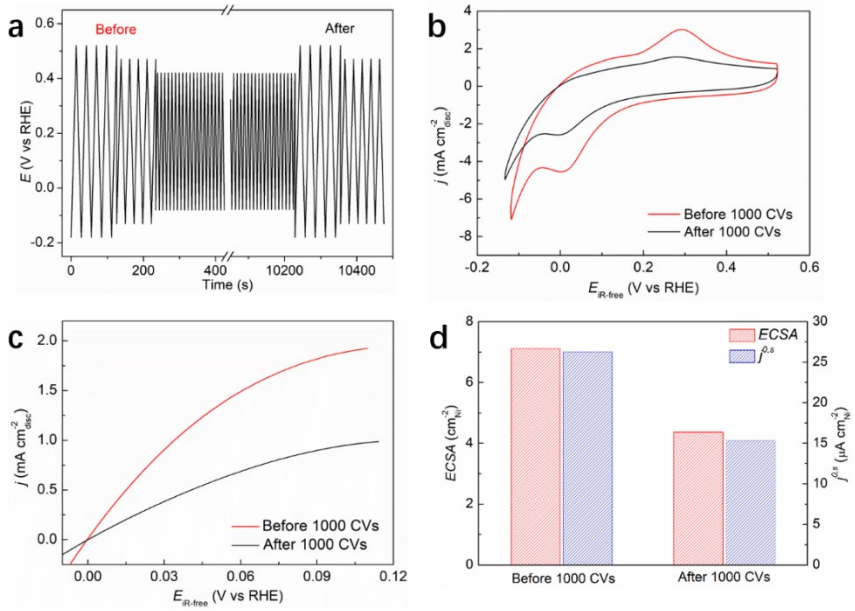

Fig. S16 Electrochemical stability tests of NiB-300. (a) Schematic protocol of the potential window during the 1000 CVs. (b) CVs in Ar-saturated 0.1 M KOH at a scan rate of 50 mV s^{-1} before and after 1000 CVs. (c) HOR polarization curves in H_2-saturated 0.1 M KOH at a rotating speed of 2500 rpm with a scan rate of 5 mV s^{-1} before and after 1000 CVs. (d) Comparison of the ECSAs and the exchange current densities before and after 1000 CVs.

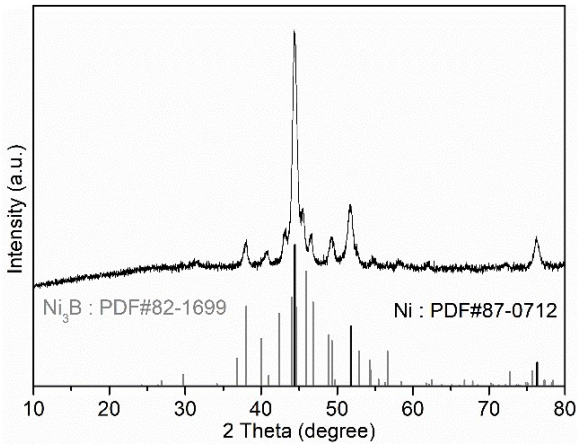

Fig. S17 XRD pattern of Ni_3B-300.

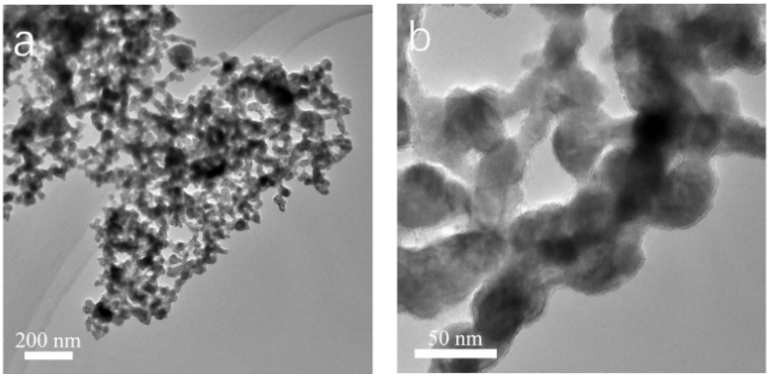

Fig. S18 TEM images of Ni_3B-300.

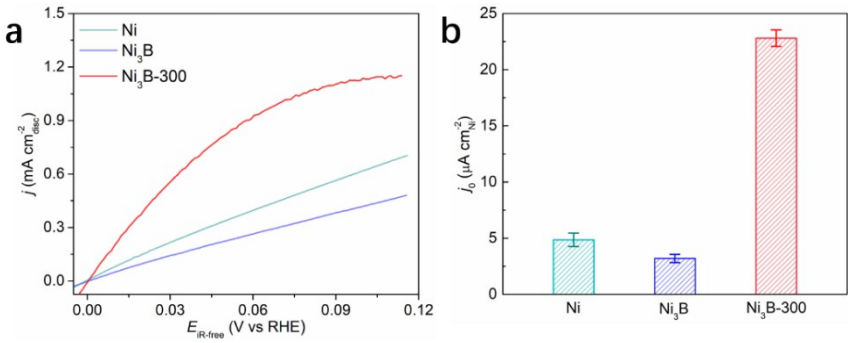

Fig. S19 (a) HOR polarization curves of Ni, Ni_3B and Ni_3B-300 recorded in H_2-saturated 0.1 M KOH at a scan rate of 5 mV s^{-1} and a rotating speed of 2500 rpm; (b) Comparison of j_0 of Ni, Ni_3B and Ni_3B-300.

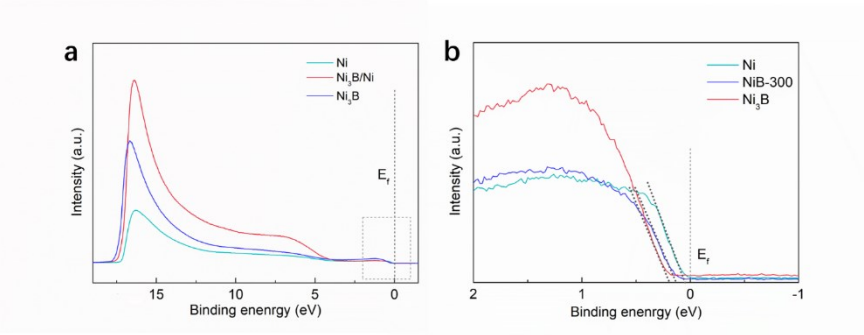

Fig. S20 UPS spectra of Ni, Ni_3B, and NiB-300 after treated by Ar^+ sputtering of 2 kV for a duration of 45 s to mitigate the surface contamination. The spectrometer is equipped with a He discharge lamp for UPS (He I at hν = 21.22 eV) with a sample bias of −10 eV and the Au $4f_{7/2}$ core-level signal at 83.8 eV binding energy was taking as the electron energy calibration reference.

The work function (ϕ) could be calculated from the following equation,

$$\phi = h_v + E_{cutoff} - E_f$$

where h_v is the energy of the UV photon (He I, 21.22 eV), E_{cutoff} is the energy of the final state, and E_f is the Fermi energy (or the energy of the initial state). Therefore, the work function of Ni (4.12 eV) is larger than that of Ni_3B (4.01 eV), which shows the same trend as our calculated results.

Besides that, the valence band maximum values are calculated to be 0.05, 0.18, and 0.12 eV of Ni, Ni_3B, and NiB-300, respectively, as shown in Fig. S20b. Compared to Ni, the valence band of NiB-300 is shifted away from the Fermi level, indicating the downshifted d-band center. Meanwhile, the valence band of NiB-300 is closer to the Fermi level than Ni_3B, indicating the upshifted d-band center. These conclusions are consistent with our calculated results (Fig. 4e and f).

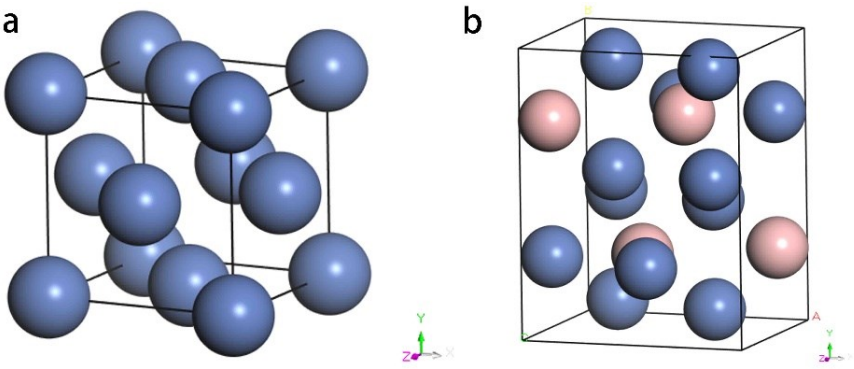

Fig. S18 The crystal structure of (a) Ni and (b) Ni_3B metal.

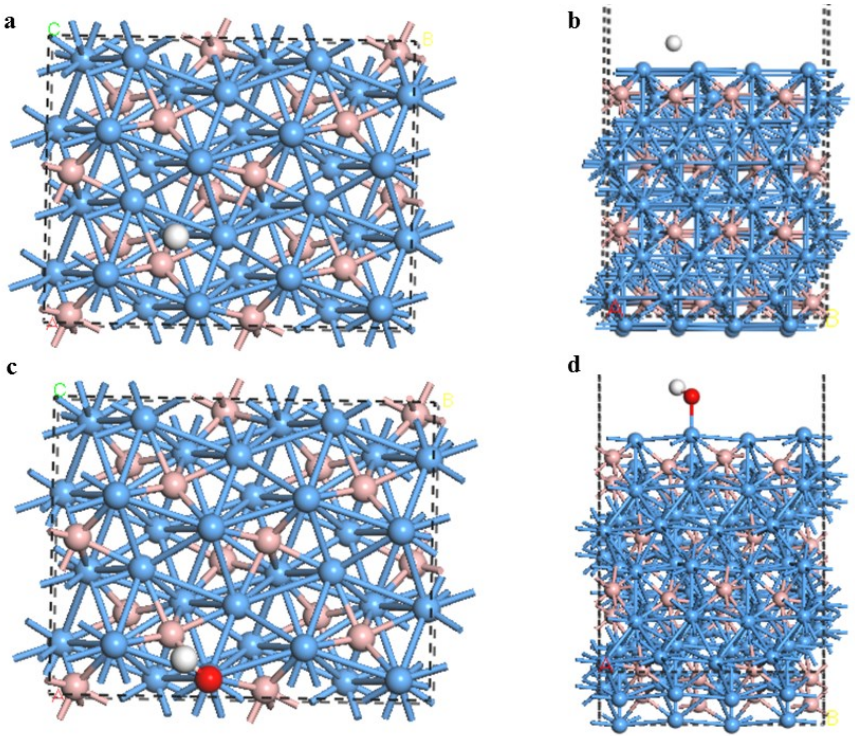

Fig. S19 The front view and the top view of (a-b) hydrogen adsorption (c-d) and the hydroxyl adsorption on Ni_3B (001) surface.

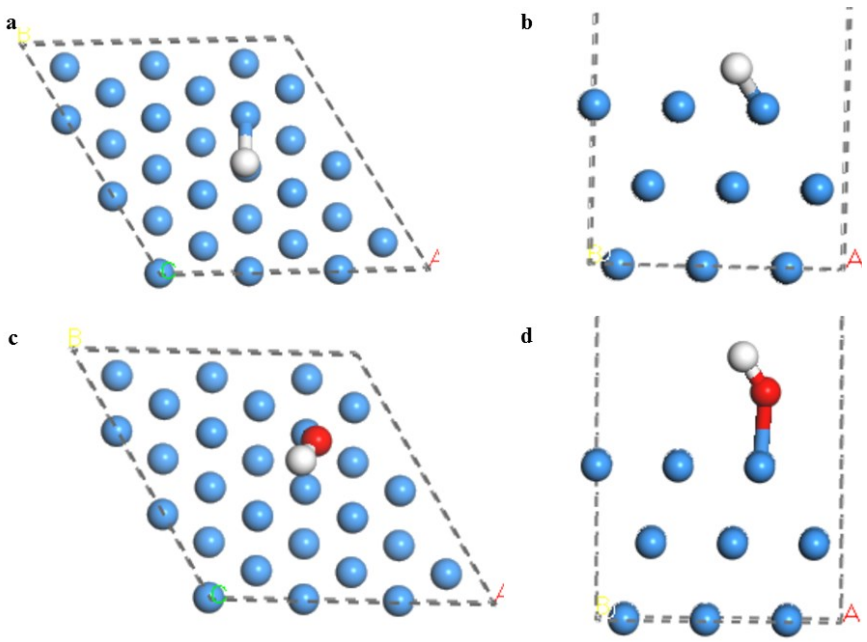

Fig. S20 The front view and the top view of (a-b) hydrogen adsorption (c-d) and the hydroxyl adsorption on Ni (111) surface.

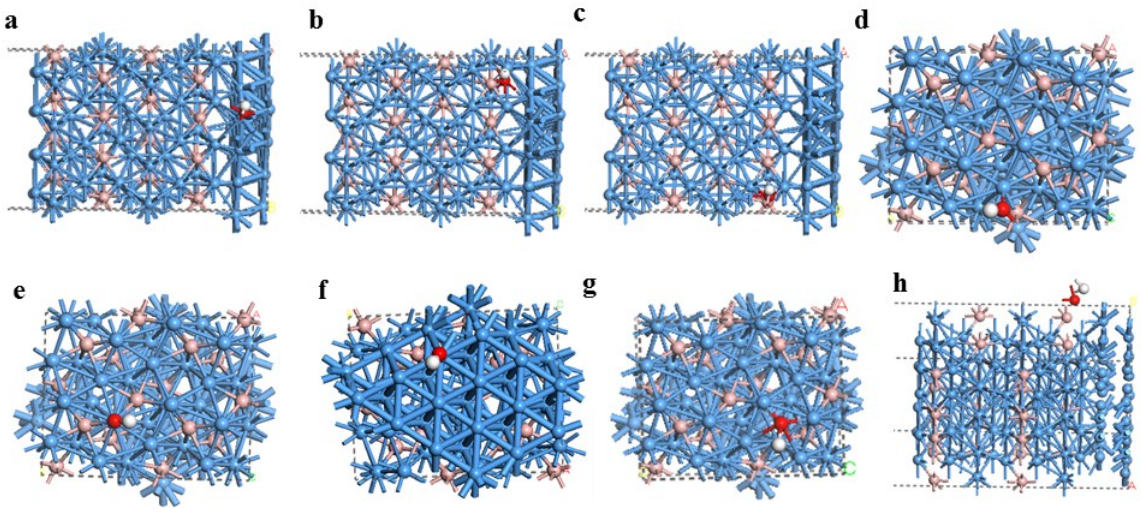

Fig. S21 The geometric configurations of the hydroxyl adsorption of Ni_3B/Ni on different sites.

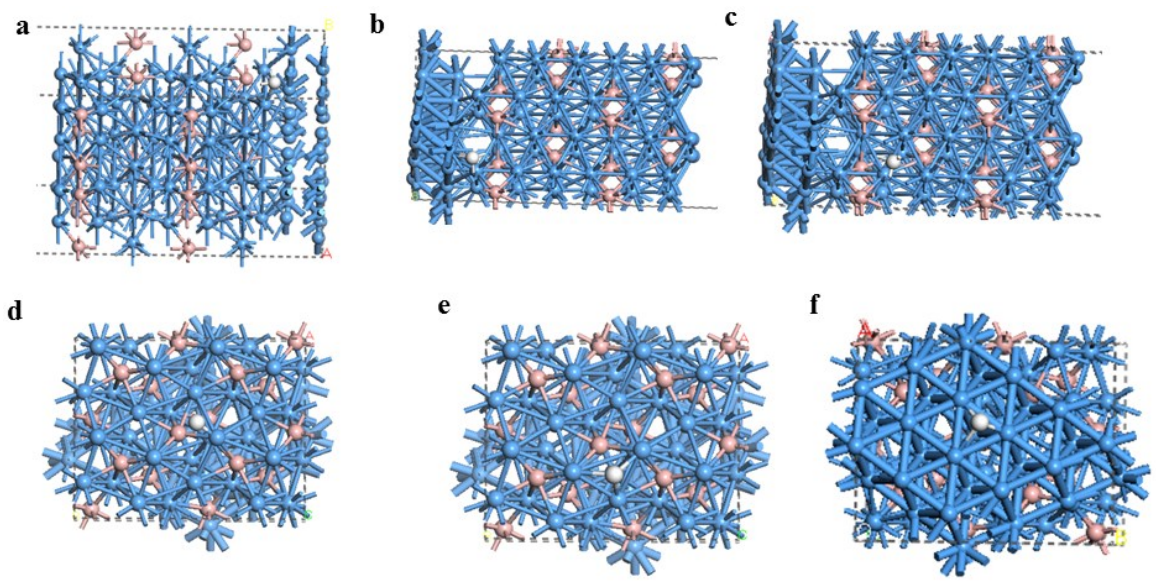

Fig. S22 The geometric configurations of the H adsorption of Ni_3B/Ni on different sites.

Table S1 ICP-AES results of amorphous Ni-B precursor, NiB-200, NiB-300 and NiB-400.

Sample	Ratio of Ni : B (atomic ratio)	Loadings on GC (mg_{Ni} cm^{-2})
Amorphous Ni-B precursor	2.108 : 1	0.141
NiB-200	2.070 : 1	0.140
NiB-300	2.048 : 1	0.140
NiB-400	4.469 : 1	0.147

Table S2 Summary of the exchange current densities and the mass activities (at the overpotential of 50 mV) of all the Ni-based catalysts in this work.

Sample	Exchange current density (μA cm_{ECSA}^{-2})	Mass activity@50 mV (mA mg_{Ni}^{-1})
NiB-300	25.37±1.33	24.71±1.67
NiB-400	19.86±2.21	10.63±1.24
NiB-200	1.37±0.15	1.18±0.12
Ni	4.85±0.59	3.91±0.36
Ni_3B	3.19±0.37	2.22±0.21
Ni_3B-300	22.85±0.74	/

Table S3 Benchmark HOR activities and the relevant parameters of the Ni-based and some Pd-based catalysts in alkaline electrolytes.

Sample	Temperature /K	Loading (mg_{Ni} cm^{-2})	$j^{0,s}$ (mA cm_{Ni}^{-2})	j^{m}@50mV (mA mg_{Ni}^{-1})	Reference
NiB-300	303	0.142	0.026	24.7	This work
NiB-400		0.147	0.020	10.6	
Ni/N-CNT	r.t.	0.25	0.028	9.3	*Nat. Commun.* **2016**, *7*, 10141
Ni/CNT			0.0092	1.9	
Ni			0.0013	0.28	
Ni_3N/C	/	0.16	0.014	24.38	*Angew. Chem. Int. Ed.* **2019**, *58*, 7445-7449
Ni_3N		0.28	0.017	1.73	
Ni-Ref		0.28	0.002	1.07	
Ni/NiO/C-700	298	0.16	0.026	5.0	*Angew. Chem. Int. Ed.* **2019**, *58*, 10644-10649
CoNiMo	293	/	0.015 (α=0.5) 0.007 (α=1.0)	/	*Energy Environ. Sci.* **2014**, *7*, 1719-1724
np-Ni_3N	298	0.16	/	29.75	*Energy Environ. Sci.* **2019**, *12*, 3522-3529
$Ni_{0.95}Cu_{0.5}$/C	298	0.025 (Ni+Cu)	0.014	/	*J. Electroanal. Chem.* **2016**, *783*, 146-151
Ni_3@ $(hBN)_1$/C-700NH_3	/	0.25	0.023	/	*Chem. Sci.* **2017**, *8*, 5728-5734
Ni/SC	303	0.138	0.040	8.6	*J. Mater. Chem. A* **2019**, *7*, 10936-10941
CeO_2(r)-Ni/C-1	303	0.141	0.038	12.28	*Angew. Chem. Int. Ed.* **2019**, *58*, 14179-14183
NiMo/KB	298	0.1 (Ni+Mo)	0.027	/	*J. Mater. Chem. A* **2017**, *5*, 24433-24443
Pd/C	/	0.02 (Pd)	0.04	/	*Sci. Adv.* **2016**, *2*, e1501602
Pd/Au	293	/	0.022	/	*J. Electrochem. Soc.* **2015**, *162*, F178-F189
Pd/CN_x	298	43 (Pd)	0.037	/	*ACS Catal.* **2016**, *6*, 1929-1941

Table S4 The corresponding OH* adsorption energy in the Figure S21.

Sample	**Ni_3B/Ni Heterostructure**							
Sites	a	b	c	d	e	f (Ni)	g	h
ΔG_{OH*} (eV)	-0.72	**-0.97**	-0.61	0.39	0.41	-0.12	-0.52	-0.86

Table S5. The corresponding H* adsorption energy in the Figure S22.

Sample	**Ni_3B/Ni Heterostructure**					
Sites	a	b	c	d	e	f
ΔG_{H*} (eV)	**-0.30**	-0.18	-0.21	-0.29	-0.21	-0.23

References

1. J. Masa, I. Sinev, H. Mistry, E. Ventosa, M. de la Mata, J. Arbiol, M. Muhler, B. R. Cuenya and W. Schuhmann, *Adv. Energy Mater.*, 2017, **7**, 1700381.

2. X. Chen, Z. Yu, L. Wei, Z. Zhou, S. Zhai, J. Chen, Y. Wang, Q. Huang, H. E. Karahan, X. Liao and Y. Chen, *J. Mater. Chem. A*, 2019, **7**, 764-774.

3. Z. Zhuang, S. A. Giles, J. Zheng, G. R. Jenness, S. Caratzoulas, D. G. Vlachos and Y. Yan, *Nat. Commun.*, 2016, **7**, 10141.

4. Z. L. Schaefer, X. Ke, P. Schiffer and R. E. Schaak, *J. Phys. Chem. C*, 2008, **112**, 19842-19851.

5. W. Sheng, H. A. Gasteiger and Y. Shao-Horn, *J. Electrochem. Soc.*, 2010, **157**, B1529-B1536.

6. R. M. Barrer and B. E. F. Fender, *J. Phys. Chem. Solids*, 1961, **21**, 12-24.

7. X. Gao, D. Chen and D. Dollimore, *Thermochim. Acta*, 1993, **223**, 75-82.